Underwater Acoustic Imaging with Spatial Cross Correlation for Weak Noise Source Identification

Hu Yang, Hang Chen, Zhanlong Yang, Yanni Gou
School of Marine Technology
Northwestern Polytechnical University
Xi'an 710072, China
yanghu@mail.nwpu.edu.cn

Jinyan Du
Institute of Oceanographic Instrumentation
Shandong Academy of Science
Qingdao 266001, China
djyjane@gmail.com

***Abstract*—A cross-correlation based imaging approach to reconstructing the intensity distribution of noise sources passively is proposed for weak noise source identification in this paper. In the proposed method, all pairs of the received noise signals from noise source radiations are cross correlated first, and then these cross-correlations are delayed-and-summed to recover the noise source image. Since cross-correlation is similar in principle to matched filtering, the proposed method offers the ability of reconstructing weak noise sources. Numerical simulations for resolution analysis and source imaging in the case of point noise source are carried out to verify the validity of the proposed method. Simulation results show that the proposed method achieves a better performance than the conventional beamforming method and not only the signal-to-noise ratio (SNR) enhancement but also the better resolution obtained with the proposed method only using relatively fewer elements.**

Keywords—underwater acoustic imaging; passive imaging; cross-correlation; weak noise source; sparse array

I. Introduction

As an acoustic visualization technique, acoustic imaging provides an effective way to identify noise sources based on source images. Passive imaging of underwater noise source enables reconstructing the source distribution with minimal disturbance to the sound field, which can localize and quantify the noise source from its noise radiations. Therefore, passive imaging is particularly useful for source identification in obtaining the source position and the source intensity.

With the benefit of simple practical realization, the beamforming-based approach to acoustic imaging [1] is a useful method in noise source identification. The delay-and-sum beamforming method in time domain is applied to impulsive sound source localization [2] and the similar approach is presented in [3] to sound source imaging of airborne targets. Meanwhile, the beamforming approach in frequency domain is applied in mobile robot for simultaneous moving sources localization [4]. Under the condition of near-field, focused beamforming with sparse array is considered in [5] to perform underwater acoustic image measurement of ships from the recorded radiated noises.

In addition to the beamforming approach, nearfield acoustical holography (NAH) [6, 7] is a celebrated technique for noise source identification. NAH can provide a more global view of noise distribution and the relative intensity. Applications of the NAH technique are performed to identify the source strength distribution of aeroacoustic sources [8] and underwater moving noise sources [9]. Besides, a nearfield equivalence source imaging (NESI) technique is proposed to reconstruct the sound field for source identification, which is essentially a unified approach of the NAH and a beamformer [10].

In practical application, the received signals radiated from the noise sources always suffer significant attenuation in water and are even masked by the presence of strong interferers. In this case, the problem of underwater noise source identification is always to be solved under the condition of low SNR. Therefore, the problem of weak noise source identification is what we consider more in practice.

Evidently, the importance of weak noise source identification is to enhance the SNR of the received noise signals. In conventional beamforming based approach, it is helpful to achieve high gain and resolution by employing a wide array aperture with a large number of elements. However, more elements also brings the heavy cost and computation burden of system. Some source localization method within a matched-field processing framework [11, 12] facilitates localization of weak sources. Actually, the weak source localization is performed by canceling the strong interferences, concentrating on interference cancellation.

In this paper, a cross-correlation based imaging approach to reconstruct the noise source distribution is proposed for weak noise source identification. The proposed approach can provide a significant improvement for weak noise source and is simply-realized and low-cost, only using a few array elements. Simulation results show that the proposed method achieve a better performance than the conventional beamforming method.

II. Acoustic Imaging with Spatial Cross Correlation

A. Motivation

As mentioned above, the problem of noise source imaging can be stated as reconstructing the intensity distribution of noise sources. Hence, our objective is to obtain the location

This work was supported by the Northwestern Polytechnical University Foundation for Fundamental Research under Grant NPU-FFRJC201226.

978-0-933957-40-4 ©2013 MTS

and intensity of noise sources. We start with obtainment of the intensity (here as average power) to develop our imaging approach.

The average power of a random process is given by

$$\frac{1}{2\pi}\int_{-\infty}^{\infty} G(\omega)\,\mathrm{d}\omega = R(\tau)\Big|_{\tau=0} \tag{1}$$

where $R(\tau)$ and $G(\omega)$ is the auto-correlation and the power spectrum density of the random process, respectively [13]. From Eq. (1), we find that the intensity of the noise source can be obtained with its auto-correlation.

A noise source located at $\boldsymbol{r}=\boldsymbol{r}_{\mathrm{s}}$ is characterized as a function of time and space, and modeled by

$$s(\boldsymbol{r},t) = f(t)\,\delta(\boldsymbol{r}-\boldsymbol{r}_{\mathrm{s}}) \tag{2}$$

where $f(t)$ is the radiated noise signal, and $s(\boldsymbol{r},t)$ is termed as source distribution [14]. Assume the radiated noise signal is a stationary random process. The auto-correlation of the source distribution $s(\boldsymbol{r},t)$ is defined by

$$\begin{aligned} R_{\mathrm{s}}(\boldsymbol{r},\tau) &= E\left[s(\boldsymbol{r}_{\mathrm{s}},t)\,s(\boldsymbol{r}_{\mathrm{s}},t+\tau)\right] \\ &= R_f(\tau)\,\delta(\boldsymbol{r}-\boldsymbol{r}_{\mathrm{s}}) \end{aligned} \tag{3}$$

where $E[\cdot]$ denotes statistical expectation and $R_f(\tau) = E\left[f(t)f(t+\tau)\right]$ is the auto-correlation of $f(t)$.

Eq. (3) formulates the problem of reconstructing the intensity distribution of noise sources. The distribution of noise sources can be expressed by auto-correlation of the source distribution in Eq. (3) which means there is a noise source in space located at $\boldsymbol{r}=\boldsymbol{r}_{\mathrm{s}}$ with its average power $R_f(0)$. If we get the auto-correlation of the source distribution, the intensity distribution of noise sources can be known. Since the recorded radiated noise signals are produced through forced injection of noise sources, the auto-correlation of the source distribution can be obtained indirectly by cross-correlating the recorded signals. In this way, our cross-correlation based imaging approach is developed.

Since cross-correlation is similar in principle to matched filtering, which is known to maximize SNR in the presence of white Gaussian noise, our approach can offer the ability of reconstructing weak noise sources.

B. Principles of cross-correlation based imaging

Consider P distributed noise sources located at positions $\boldsymbol{r}_p\ (p=1,\cdots,P)$ and an M-element planar array with an arbitrary geometry. Assume noise sources are isotropic, spatially incoherent, and located in the same plane. The coordinates system for noise sources, array, and the region of interest to be imaged is depicted in Fig. 1.

The pth noise source distribution can be written as

$$s_p(\boldsymbol{r},t) = f_p(t)\,\delta(\boldsymbol{r}-\boldsymbol{r}_p) \tag{4}$$

where $f_p(t)$ is the radiated noise signal from the pth noise source. The auto-correlation of the pth noise source distribution is

$$R_{s_p}(\boldsymbol{r},\tau) = R_{f_p}(\tau)\,\delta(\boldsymbol{r}-\boldsymbol{r}_p) \tag{5}$$

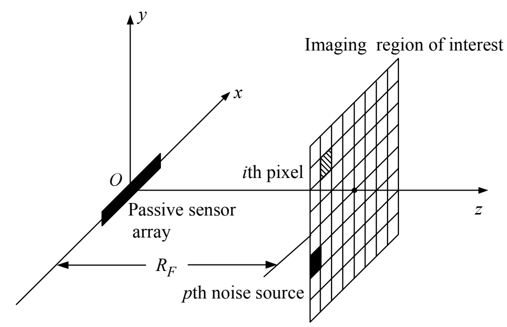

Fig. 1. The coordinates system for noise source, array, and the imaging region.

The recorded radiated noise signal at the mth array element is

$$x_m(\boldsymbol{r}_m,t) = \sum_{p=1}^{P} \frac{1}{\left|\boldsymbol{r}_m-\boldsymbol{r}_p\right|} f_p\left(t-\left|\boldsymbol{r}_m-\boldsymbol{r}_p\right|/c\right) \tag{6}$$

where $\left|\boldsymbol{r}_m-\boldsymbol{r}_p\right|$ is the distance between the pth noise source and the mth element.

To obtain Eq. (5), we cross-correlate any pair of the recorded noise signals, that is

$$R_{x_m x_n}(\boldsymbol{r}_m,\boldsymbol{r}_n,\tau) = E\left[x_m(\boldsymbol{r}_m,t)\,x_n(\boldsymbol{r}_n,t+\tau)\right] \tag{7}$$

where $R_{x_m x_n}(\boldsymbol{r}_m,\boldsymbol{r}_n,\tau)$ is the cross-correlation between the mth and the nth element.

Substituting Eq. (6) into Eq. (7) and considering noise sources are uncorrelated results in

$$\begin{aligned} R_{x_m x_n}(\boldsymbol{r}_m,\boldsymbol{r}_n,\tau) &= E\left\{\left[\sum_{p=1}^{P}\frac{1}{\left|\boldsymbol{r}_m-\boldsymbol{r}_p\right|} f_p\left(t-\left|\boldsymbol{r}_m-\boldsymbol{r}_p\right|/c\right)\right]\right. \\ &\qquad \left.\times\left[\sum_{p=1}^{P}\frac{1}{\left|\boldsymbol{r}_n-\boldsymbol{r}_p\right|} f_p\left(t+\tau-\left|\boldsymbol{r}_n-\boldsymbol{r}_p\right|/c\right)\right]\right\} \\ &= \sum_{p=1}^{P}\frac{1}{\left|\boldsymbol{r}_m-\boldsymbol{r}_p\right|\left|\boldsymbol{r}_n-\boldsymbol{r}_p\right|} E\left[f_p\left(t-\left|\boldsymbol{r}_m-\boldsymbol{r}_p\right|/c\right)\right. \\ &\qquad \left.\times f_p\left(t+\tau-\left|\boldsymbol{r}_n-\boldsymbol{r}_p\right|/c\right)\right] \\ &= \sum_{p=1}^{P}\frac{1}{\left|\boldsymbol{r}_m-\boldsymbol{r}_p\right|\left|\boldsymbol{r}_n-\boldsymbol{r}_p\right|} R_{f_p}\left(\tau-\frac{\left|\boldsymbol{r}_n-\boldsymbol{r}_p\right|-\left|\boldsymbol{r}_m-\boldsymbol{r}_p\right|}{c}\right) \end{aligned} \tag{8}$$

In this way, $M(M-1)$ cross-correlation functions can be obtained with cross-correlating the recorded noise signals from all pairs of elements. Then, the generated image of the region of interest, on the basis of $M(M-1)$ cross-correlation functions, is given by

$$Image(\boldsymbol{r}_i) = \frac{1}{M(M-1)}\sum_{m=1}^{M}\sum_{\substack{n=1\\ n\neq m}}^{M} \left|\boldsymbol{r}_i-\boldsymbol{r}_m\right|\left|\boldsymbol{r}_i-\boldsymbol{r}_n\right| R_{x_m x_n}\left(\boldsymbol{r}_m,\boldsymbol{r}_n,\tau(\boldsymbol{r}_i)\right) \tag{9}$$

where

$$\boldsymbol{r}_i = (x_i, y_i, R_F),\ (i=1,\cdots,I) \tag{10}$$

is the ith pixel of the imaging region, $|\boldsymbol{r}_i - \boldsymbol{r}_m|$ is the distance between the ith pixel and the mth element, $|\boldsymbol{r}_i - \boldsymbol{r}_n|$ is the distance between the ith pixel and the nth element, and

$$\tau(\boldsymbol{r}_i) = \frac{|\boldsymbol{r}_i - \boldsymbol{r}_m| - |\boldsymbol{r}_i - \boldsymbol{r}_n|}{c} \tag{11}$$

is the time delay from the ith pixel to the mth and nth element. $|\boldsymbol{r}_i - \boldsymbol{r}_m||\boldsymbol{r}_i - \boldsymbol{r}_n|$ is to compensate for spherical spreading losses.

To verify the imaging algorithm described by Eq. (9), first all noise sources are assumed as white Gaussian noises to simplify the derivation, and then $R_{f_p}(\tau)$ in Eq. (5) reduces to

$$R_{f_p}(\tau) = \sigma_{f_p}^2 \delta(\tau) \tag{12}$$

where $\sigma_{f_p}^2$ denotes the variance of $f_p(t)$. Thus, Eq. (8) becomes

$$R_{x_m x_n}(\boldsymbol{r}_m, \boldsymbol{r}_n, \tau) = \sum_{p=1}^{P} \frac{1}{|\boldsymbol{r}_m - \boldsymbol{r}_p||\boldsymbol{r}_n - \boldsymbol{r}_p|} \sigma_{f_p}^2 \times \delta\left(\tau - \frac{|\boldsymbol{r}_n - \boldsymbol{r}_p| - |\boldsymbol{r}_m - \boldsymbol{r}_p|}{c}\right) \tag{13}$$

In Eq. (13), when $\tau(\boldsymbol{r}) = \tau(\boldsymbol{r}_p)\ (p = 1, \cdots, P)$

$$\delta\left(\tau - \frac{|\boldsymbol{r}_n - \boldsymbol{r}_p| - |\boldsymbol{r}_m - \boldsymbol{r}_p|}{c}\right)\Bigg|_{\tau(\boldsymbol{r}) = \tau(\boldsymbol{r}_p)} = \delta(0) \tag{14}$$

and when $\tau(\boldsymbol{r}) \neq \tau(\boldsymbol{r}_p)\ (p = 1, \cdots, P)$

$$\delta\left(\tau - \frac{|\boldsymbol{r}_n - \boldsymbol{r}_p| - |\boldsymbol{r}_m - \boldsymbol{r}_p|}{c}\right)\Bigg|_{\tau(\boldsymbol{r}) \neq \tau(\boldsymbol{r}_p)} = 0 \tag{15}$$

It means the cross-correlation between the mth and the nth element has values $\sigma_{f_p}^2 \delta(0)$ at $\boldsymbol{r} = \boldsymbol{r}_p\ (p = 1, \cdots, P)$ and zero values at others, which can be expressed as $\sigma_{f_p}^2 \delta(0) \delta(\boldsymbol{r} - \boldsymbol{r}_p)$. Thus, Eq. (13) can be rewritten as

$$R_{x_m x_n}(\boldsymbol{r}_m, \boldsymbol{r}_n, \tau(\boldsymbol{r})) = \sum_{p=1}^{P} \frac{1}{|\boldsymbol{r}_m - \boldsymbol{r}_p||\boldsymbol{r}_n - \boldsymbol{r}_p|} \sigma_{f_p}^2 \delta(0) \delta(\boldsymbol{r} - \boldsymbol{r}_p) \tag{16}$$

Substituting Eq. (16) into Eq. (9) yields

$$\begin{aligned} Image(\boldsymbol{r}) &= \frac{1}{M(M-1)} \sum_{m=1}^{M} \sum_{\substack{n=1 \\ n \neq m}}^{M} \sum_{p=1}^{P} \sigma_{f_p}^2 \delta(0) \delta(\boldsymbol{r} - \boldsymbol{r}_p) \\ &= \sum_{p=1}^{P} \sigma_{f_p}^2 \delta(0) \delta(\boldsymbol{r} - \boldsymbol{r}_p) \end{aligned} \tag{17}$$

From Eq. (17), it can be known that, when one of the pixels, denoted as the ith pixel, is located at the position of one of the noise sources, denoted as the P_1th noise source, there will be a highlight point located at $\boldsymbol{r}_i = \boldsymbol{r}_{P_1}$ in the generated image. The intensity of the highlight point is the average power of the P_1th noise source $\sigma_{f_p}^2 \delta(0)$. The acoustic responses of all pixels can be obtained with Eq. (9). Disregarding reverberation, if a given pixel contains a noise source, it shows a highlight point at the corresponding position representing the existence of the noise source with its intensity, and if does not contains any noise source, its acoustic response is null. In this way, the intensity distribution of noise sources is known from the generated image. Evidently, Eq. (17) shows that the reconstruction of noise sources can be obtained by the cross-correlation based imaging approach.

As mentioned above, Eq. (17) is obtained with the condition of white noises. Actually, the noise sources are always considered as band-limited noises. In this case, in Eq. (8), when $\tau(\boldsymbol{r}) = \tau(\boldsymbol{r}_p)\ (p = 1, \cdots, P)$

$$R_{f_p}\left(\tau - \frac{|\boldsymbol{r}_n - \boldsymbol{r}_p| - |\boldsymbol{r}_m - \boldsymbol{r}_p|}{c}\right)\Bigg|_{\tau(\boldsymbol{r}) = \tau(\boldsymbol{r}_p)} = R_{f_p}(0) \tag{18}$$

and

$$R_{f_p}\left(\tau - \frac{|\boldsymbol{r}_n - \boldsymbol{r}_p| - |\boldsymbol{r}_m - \boldsymbol{r}_p|}{c}\right)\Bigg|_{\tau(\boldsymbol{r}) \neq \tau(\boldsymbol{r}_p)} = R_{f_p}(\tau)\Big|_{\tau \neq 0} \tag{19}$$

at other positions. Unlike white noises, the generated image of band-limited noises shows a highlight region, not a point, at the position of the noise source.

III. Simulations

Numerical simulations are conducted to verify the theory and to demonstrate the performance of our imaging method. The resolution of our imaging method is analyzed firstly, and then the imaging simulations are carried out in the case of point noise source considering scenarios containing the absence and presence of background noise.

A. Resolution analysis

We analyze the resolution of our imaging method by numerical simulation qualitatively. We focus our analysis on the impact of the bandwidth of the radiated noise signals and the effective aperture of the array.

1) Impact of bandwidth

Consider a 5-element uniform linear array with 0.3 m element spacing. Assume the distance between the array and the imaging region $R_F = 10$ m . Fig. 2 shows the impact of bandwidth B on lateral resolution.

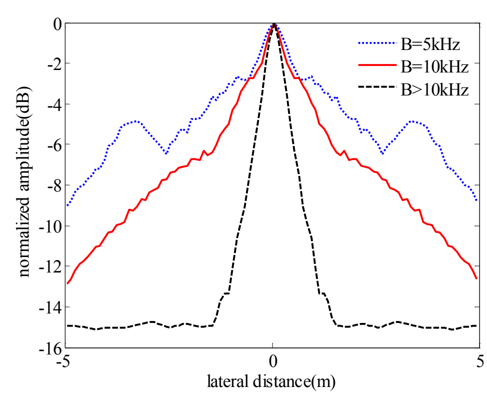

Fig. 2. Bean pattern of the proposed method in the case of $B = 5$ kHz , $B = 10$ kHz , and $B > 10$ kHz .

From Fig. 2, we can see the wider the bandwidth, the better the resolution. In simulation, the 3-dB resolutions for three cases are 1.88 m, 1.42 m, and 0.42 m, respectively. In addition to resolution improvement, it is beneficial for sidelobe reduction by increasing bandwidth. As shown in Fig. 2, the height of the sidelobes decrease as the bandwidth increases.

2) Impact of effective aperture

Consider a 5-element uniform linear array with adjustable element spacing. Assume $R_F = 10$ m and $B > 10$ kHz . Fig. 3 shows the impact of effective aperture L on lateral resolution.

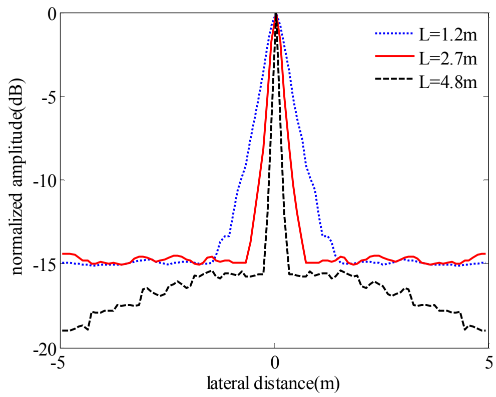

Fig. 3. Bean pattern of the proposed method in the case of $L = 1.2$ m , $L = 2.7$ m , and $L = 4.8$ m .

Similarly, from Fig. 3, we can see the larger the effective aperture, the better the resolution. The 3-dB resolutions for three cases are 0.42 m, 0.18 m, and 0.01 m, respectively. Evidently, the effective aperture is enlarged simply by increasing the element spacing and such an array is referred to as a sparse array. Thus, only a few elements can be adopted to achieve a good resolution with the proposed method.

B. Imaging in the absence of background noise

Consider a uniform planar array with 5×5 elements and 0.3 m element spacing. Assume the noise source is a Gaussian distributed point source with mean $m = 0$ and variance $\sigma^2 = 1$. We fix the imaging region in the domain $[-5,5] \times [-5,5]$ m^2 with each pixel 0.1×0.1 m^2 . The centers of the array and the imaging region are located at $(0,0,0)$ m and $(0,0,-20)$ m .

First, we choose a single point noise source located at $(0,0,-20)$ m with $B > 10$ kHz . Fig. 4 and Fig. 5 show the simulated images of the noise source obtained with the proposed method and the conventional beamforming method, respectively. For comparison, the beam patterns on the plane $Y = 0$ m of two methods are shown in Fig. 6.

Fig. 7 shows the images of two uncorrelated point sources with the same intensity, located at $(-3,1,-20)$ m and $(2,0,-20)$ m , respectively.

From Fig. 4 and Fig. 5, it can be seen that a better image of noise source is provided with the proposed method. Since the noise source is not an exact white noise and the pixel is smaller than the resolution, the image reveals the shape of a highlight region in the position of the noise source, not a point.

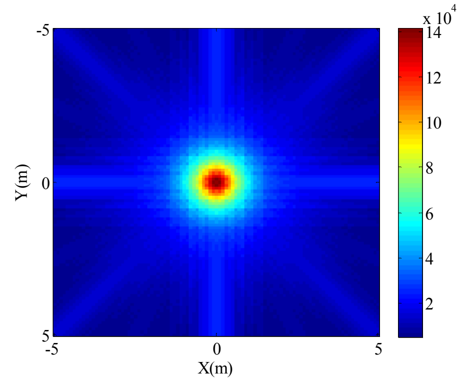

(a)

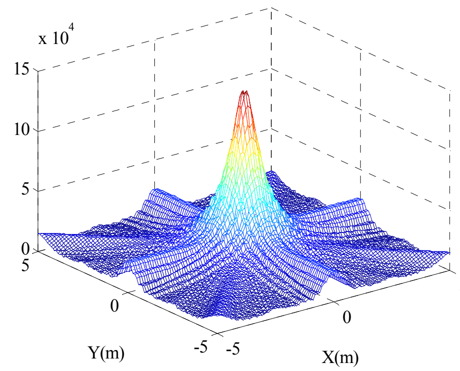

(b)

Fig. 4. Images of a single point noise source obtained with the proposed method: (a) 2-D view; (b) 3-D view.

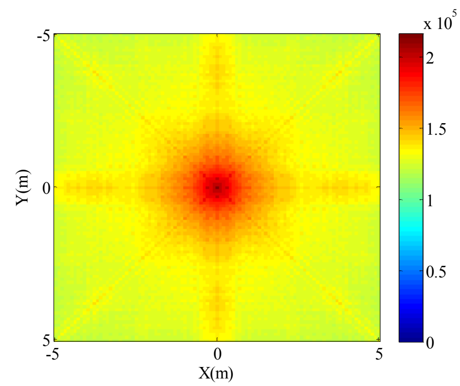

(a)

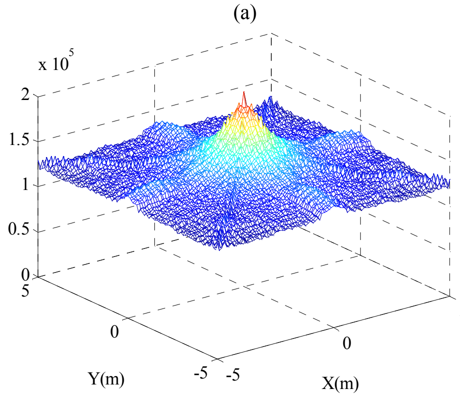

(b)

Fig. 5. Images of a single point noise source obtained with the conventional method: (a) 2-D view; (b) 3-D view.

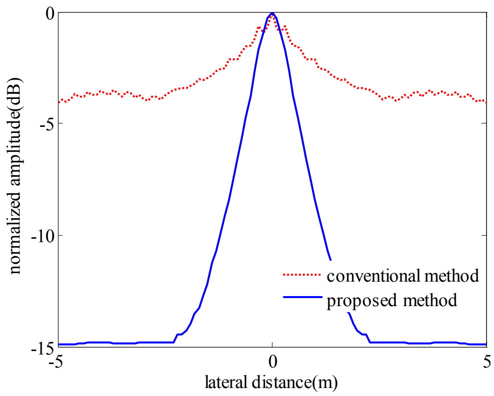

Fig. 6. Comparision of beam patterns between the proposed method and the conventional method on the plane $Y = 0$ m.

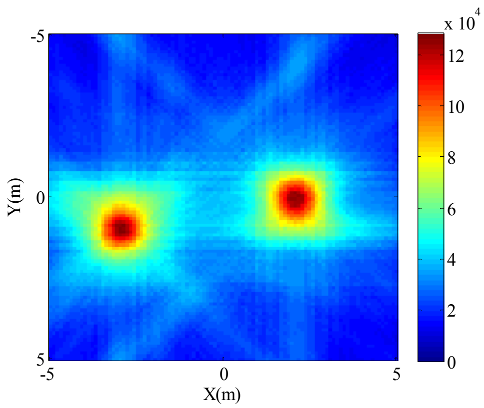

Fig. 7. Image of two uncorrelated point noise sources located at (-3, 1) m and (2, 0) m in the X-Y plane.

In Fig. 6, we can also find that the proposed method gives a good resolution of the noise source. Comparison with the conventional method shows that the mainlobe is narrower and the sidelobe is lower in the beam pattern of the proposed method. This is due to the fact the proposed method can achieve a good resolution only employing a few elements, while the conventional method leads to a poor resolution with not enough elements.

C. Imaging in the presence of background noise

In the above section, simulations are conducted in the absence of background noise, only with the radiated noise signal from the noise source. Secondly, we consider the case when the noise source is in the background noise environment.

Fig. 8 shows the image of the noise source in white Gaussian background noise under $SNR = -15\,\mathrm{dB}$. Here, other simulation condition is the same as Fig. 4.

As shown in Fig. 8, even under the condition of much lower SNR, the proposed method achieves superior performance and still provides a clear source image. As anticipated, the proposed method provides a further significant SNR improvement for the weak noise source reconstruction. The SNR improvement results from the cross-correlation operation in the proposed method. Consequently, the cross-correlation approach offers the ability of reconstructing relatively weak sources whose radiated noise level are below the background noise level.

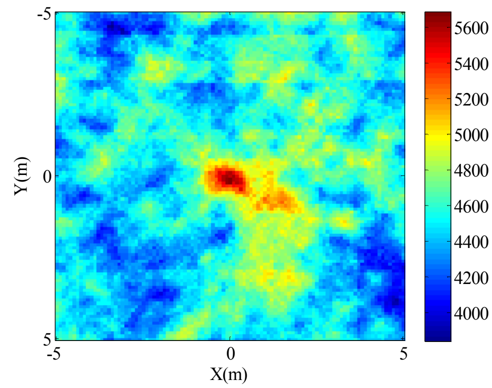

Fig. 8. Image of a single point noise source in the case of $SNR = -15\,\mathrm{dB}$.

IV. DISCUSSIONS

In this paper, a novel approach with spatial cross-correlation to underwater noise source imaging is proposed for weak noise identification. The principles of the cross-correlation based imaging are presented and some simulations are carried out. Compared with the conventional method, the advantages of the proposed method are shown as follows:

(1) The proposed method is simply-realized and low-cost, only with relatively fewer elements than the conventional method.

(2) The wider the bandwidth and the larger the effective aperture, the better the resolution. The effective aperture can be enlarged simply by increasing the element spacing.

(3) The cross-correlation operation not only provides additional SNR improvement but also performs better resolution than the conventional method.

It is noticed that the formulas for the imaging algorithm have been derived for the ideal case of isotropic and spatially incoherent random sources. When these conditions are not satisfied, source images can still be constructed by the proposed method, and pre-whitening the recorded noise signals helps improving resolution.

REFERENCES

[1] V. Murino and A. Trucco, "Three-dimensional image generation and processing in underwater acoustic vision," Proc. IEEE, vol. 88, no. 12, pp. 1903-1946, December 2000.

[2] D. H. Seo and Y. H. Kim, "Impulsive sound source localization using delay and sum beamforming method in time domain, " in Proc. Inter Noise 2010, Lisboa: SPA, 2010, pp. 5473–5482.

[3] J. Valin, F. Michaud, B. Hadjou, and J. Rouat, "Localization of simultaneous moving sound sources for mobile robot using a frequency-domain steered beamformer approach," in Proc. IEEE Int. Conf. Rob. Autom., vol. 1, 2004, pp. 1033–1038.

[4] T. S. Brandes and R. H. Benson, "Sound source imaging of low-flying airborne targets with an acoustic camera array," Appl. Acoust., vol. 68, no. 7, pp. 752–765, July 2007.

[5] J. Mei, X. Sheng, L. Guo, and J. Yin, "Sea trial research on multi-source underwater acoustic image measurement technology based on the sparse

array," in OCEANS 2010 MTS/IEEE Seattle, Piscataway: IEEE Computer Sciety, 2010, pp.1–5.

[6] J. D. Maynard, E. G. Williams, and Y. Lee, "Nearfield acoustic holography: I. Theory of generalized holography and the development of NAH," J. Acoust. Soc. Am., vol. 78, no. 4, pp. 1395–1413, April 1985.

[7] W. A. Veronesi and J. D. Maynard, "Nearfield acoustic holography (NAH) II. Holographic reconstruction algorithms and computer implementation," J. Acoust. Soc. Am., vol. 81, no. 5, pp. 1307–1322, May 1987.

[8] M. Lee, J. S. Bolton, and L. Mongeau, "Application of cylindrical near-field acoustical holography to the visualization of aeroacoustic sources," J. Acoust. Soc. Am., vol. 114, no. 2, pp. 842–858, February 2003.

[9] B. Hu and D. Yang, "Underwater moving noise sources identification based on acoustic holography," in Proc. IEEE Int. Conf. Intelligent Comput. Intelligent Syst., vol. 3, Piscataway: IEEE Computer Sciety, 2010, pp.702–705.

[10] M. R. Bai and J. Lin, "Source identification system based on the time-domain nearfield equivalence source imaging: Fundamental theory and implementation," J. Sound Vibr., vol. 307, no. 1–2, pp. 202-225, October 2007.

[11] Z. H. Michalopoulou, "Multiple source localization using a maximum *a posteriori* Gibbs sampling approach," J. Acoust. Soc. Am., vol. 120, no. 5, pp. 2627–2634, May 2006.

[12] H. C. Song, J. de Rosny, and W. A. Kuperman, "Improvement in matched field processing using the CLEAN algorithm," J. Acoust. Soc. Am., vol. 113, no. 3, pp. 1379–1386, March 2003.

[13] S. Miller and D. Childers, Probability and Random Processes: With Applications to Signal Processing and Communications. New York: Academic Press, 2004.

[14] F. B. Jensen, W. A. Kuperman, M. B. Porter, and H. Schmidt, Computational Ocean Acoustics. New York: Springer, 2011.